DOI: 10.1002/smll.200500210

Beaklike SnO_2 Nanorods with Strong Photoluminescent and Field-Emission Properties

Jr H. He, Te H. Wu, Cheng L. Hsin, Kun M. Li, Lih J. Chen, Yu L. Chueh, Li J. Chou, and Zhong L. Wang*

***B**eaklike SnO_2 nanorods were synthesized by a vapor–liquid–solid approach using Au as a catalyst. The nanorods grow along the [10$\bar{1}$] direction and the beak is formed by switching the growth direction to [1$\bar{1}\bar{2}$] through controlling the growth conditions at the end of the synthesis. The photoluminescence (PL) spectrum of the nanorods exhibits visible light emission with a peak at 602 nm. The field-emission (FE) properties of the nanorods have been measured to exhibit a turn-on field of 5.8 V μm^{-1}. A comparative study of FE measurements between SnO_2 nanorods with uniform diameters and these beaklike nanorods suggests that the shape and curved tips are important factors in determining the FE properties.*

Keywords:
- electron microscopy
- field emission
- nanorods
- photoluminescence
- tin oxide

1. Introduction

One-dimensional (1D) and quasi-one-dimensional (quasi-1D) nanostructures are attracting a great deal of attention due to their unique properties and novel applications.[1,2] Oxides are the basis of smart and functional materials that have tunable properties and important technological applications. Functional oxides have two structural characteristics: cations with mixed valence states, and anions with deficiencies (vacancies). By varying either or both of these characteristics, the electrical, optical, magnetic, and chemical properties can be modified, giving the possibility of fabricating smart devices that utilize the semiconductivity, superconductivity, ferroelectricity, and/or magnetism offered by the oxides.[3] SnO_2 is an n-type semiconducting oxide with a wide bandgap ($E_g = 3.6$ eV at 300 K) and well known for its potential applications in dye-based solar cells,[4] semiconductors,[5] photoconductors,[6] and gas sensors.[7–9] A variety of 1D and quasi-1D functional nanostructures of SnO_2 have been successfully fabricated, including nanobelts, nanowires, nanotubes, nano-box-beams, and nanodiskettes.[5–13] The promise that nanostructures may dramatically improve the desired properties for many applications has stimulated great enthusiasm.

In the present study, the optical applications of SnO_2 nanorods with a beaklike growth front are explored. The photoluminescence (PL) spectrum of such nanorods exhibits a strong emission peak at 602 nm. The field-emission properties of the SnO_2 nanorods were measured for the first time, showing a turn-on field of 5.8 V μm^{-1}. The effect of shape of SnO_2 nanostructures on the field emission properties has been fully investigated. Theoretical calculation has been carried out to find out whether there is a correlation between surface energy change and the morphological evolution.

[*] J. H. He, T. H. Wu, C. L. Hsin, K. M. Li, Prof. L. J. Chen, Y. L. Chueh, Prof. L. J. Chou
Department of Materials Science and Engineering
National Tsing Hua University, Hsinchu 300 (Taiwan)
Fax: (+886) 3571-8328
E-mail: ljchen@mx.nthu.edu.tw
Prof. Z. L. Wang
School of Materials Science and Engineering
Georgia Institute of Technology
Atlanta, Georgia 30332-0245 (USA)

Supporting information for this article is available on the WWW under http://www.small-journal.com or from the author.

NANO MICRO small

2. Results and Discussion

The first set of samples were cooled down to room temperature with a 150 sccm Ar flow and a 12.5 sccm oxygen flow, and another set of samples were cooled to room temperature with only a 150 sccm Ar flow. The structure of the as-grown nanorods was determined by XRD. As shown in Figure 1, all of the diffraction peaks for both sets of samples

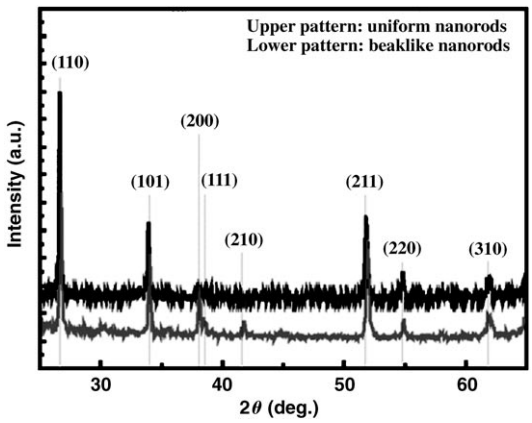

Figure 1. XRD pattern recorded from the as-synthesized products.

can be ascribed to the tetragonal rutile SnO_2 structure with lattice constants of $a = 0.4742$ nm and $c = 0.3182$ nm, consistent with the standard data file (ICDD-PDF41–1445). As shown in Figure 2a, a typical low-magnification SEM image indicates that the as-synthesized products consist of a large quantity of 1D nanostructures. The stems of the SnO_2 nanorods have diameters of 85–400 nm and lengths up to ≈20 μm. The beaklike nanostructures are typically 100–700 nm in length. A representative medium-magnification SEM image of several curved SnO_2 nanorods, as shown in Figure 2b and c, reveals that their geometrical shape is

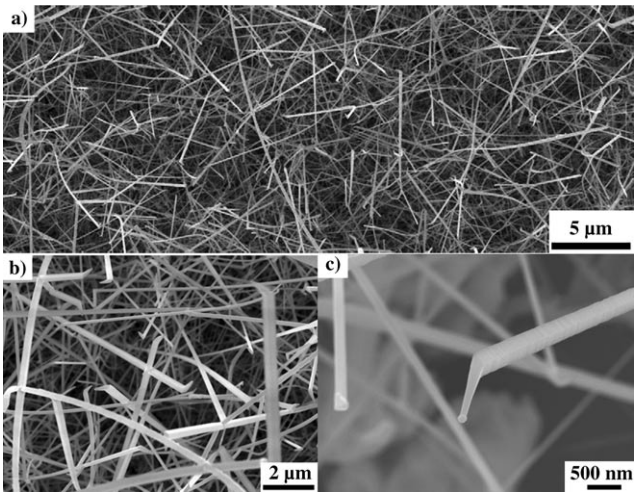

Figure 2. Typical SEM images of the as-synthesized product: a) low-magnification image; b) medium-magnification image of several beaklike nanorods with curved tips; c) high-magnification image of the beaklike nanorods.

beaklike towards the growth front, which is distinct from other previously reported SnO_2 nanostructures.[5–13] On the other hand, the stems of the curved nanorods appear to be uniform in size.

The nanostructures were further characterized with TEM and HRTEM. Figure 3a shows a typical TEM image of a single SnO_2 nanorod with a diameter of 85 nm. The corresponding selected-area electron diffraction (SAED) pattern (Figure 3b) confirms that the phase of the beaklike nanorods is of the tetragonal rutile structure. Figure 3c is a HRTEM image from the outlined region marked in Figure 3a, which indicates that the nanorods are single crystalline and free of defects. The measured lattice spacing of 0.33 nm and 0.23 nm are consistent with the d values of the (110) and $(1\bar{1}\bar{1})$ planes. The growth direction was obtained from analysis of the diffraction pattern using the concept of the reciprocal lattice. From both the diffraction pattern and the atomic image, the lattice planes of $(20\bar{1})$ and $(1\bar{1}\bar{1})$ are obtained. The corresponding normal directions $[h_1k_1l_1]$ and $[h_2k_2l_2]$ are $[h_1k_1l_1] = [20\bar{2}.3] \approx [10\bar{1}]$ and $[h_2k_2l_2] = [1\bar{1}2.3] \approx [1\bar{1}\bar{2}]$. In other words, the $[10\bar{1}]$ and $[1\bar{1}\bar{2}]$ directions are perpendicular to the $(20\bar{1})$ and $(1\bar{1}\bar{1})$ planes, respectively. (see Supporting Information)

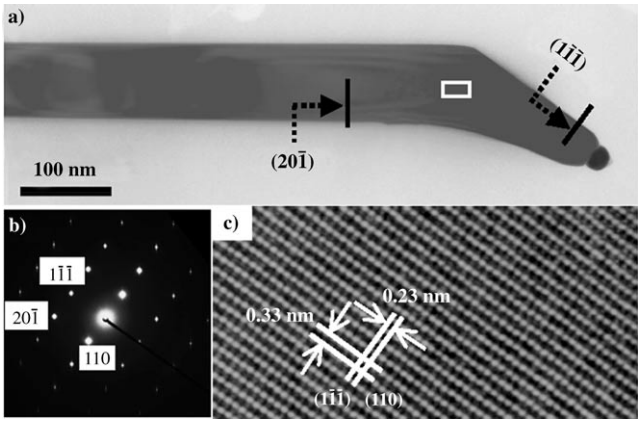

Figure 3. a) TEM image of a single beaklike SnO_2 nanorod; b) the corresponding selected-area electron diffraction (SAED) pattern; c) HRTEM image from the nanorod shown in (a).

The samples cooled to room temperature with only a 150 sccm Ar flow show a slightly different morphology. As seen in Figure 4a, the low-magnification SEM image shows that the as-synthesized products consist of a large quantity of SnO_2 nanorods. High-magnification SEM shows that the nanorods have no beaklike structure and that the Au catalysts are at the side surface rather than at the very growth front, as indicated in the inset in Figure 4a. The nanorod grows along a direction close to $[10\bar{1}]$ without subsequent growth along $[1\bar{1}\bar{2}]$ (Figure 4b). The growth of beaklike nanostructures was initiated with oxygen that remained in the furnace but could not be sustained since the oxygen flow was turned off during the cooling-down period. The presence of Au catalysts at the side surface indicates that the growth is at a stage where the beaklike tip was just beginning to grow.

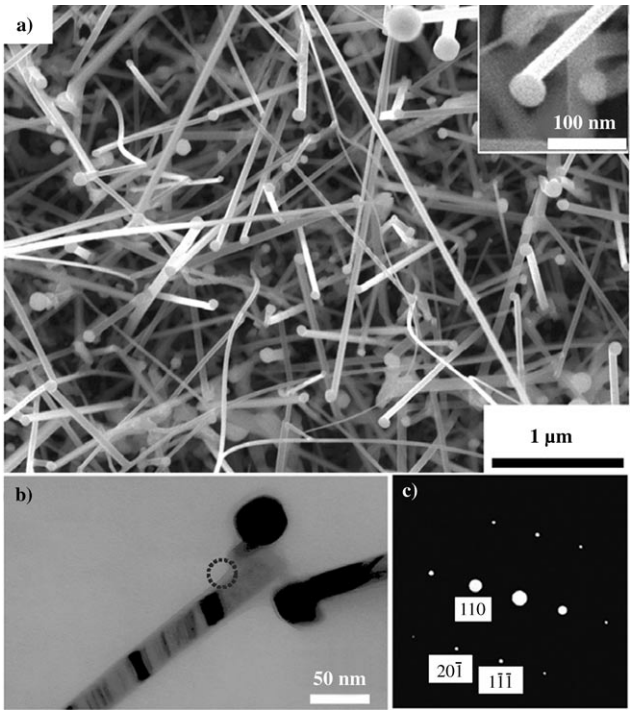

Figure 4. a) SEM image and b) TEM image of samples cooled to room temperature with only a 150 sccm Ar flow after maintaining the reaction temperature for 1 h with a 150 sccm Ar flow and a 12.5 sccm oxygen flow after the VLS process.

Theoretical calculations have been carried out to ascertain whether there is a correlation between surface energy change and morphological evolution. The surface energy, E_{surf}, is defined as the excess surface free energy per unit area of a particular crystal face, E_{surf} (hkl). The variation of this parameter with surface orientation determines the three-dimensional equilibrium crystal shape.[14] The equilibrium shape can be directly derived from the surface energies by the Wulff construction,[15] in which the distance to the center of a crystal of each face is proportional to its surface energy. Among the various planes of the rutile structure of SnO_2, the surface energies of the $(20\bar{1})$ and $(1\bar{1}\bar{1})$ planes are about 1.63 and 2.21 ($J\,m^{-2}$), respectively.[16–18] For the formation of facets B of orientation ($h_2k_2l_2$), and energy (per unit area) E^{B}_{surf}, on a surface A of orientation ($h_1k_1l_1$), and energy E^{A}_{surf} depending on the sign of the formation energy:

$$\Delta G = E^{A}_{surf}(h_1k_1l_1)\cos\theta - E^{B}_{surf}(h_2k_2l_2) \quad (1)$$

where θ is the angle between the A and B planes. The factor cosθ takes into account the change in surface area if facets were formed. The contribution of edges and vertices are neglected. If the above expression is positive ($\Delta G > 0$), surface A is not thermodynamically stable and the growth of facet B on A is feasible. On the other hand, if it is negative ($\Delta G < 0$), facets B cannot be formed.[16] If one considers the stability of the $(20\bar{1})$ surface, and the formation of a $(1\bar{1}\bar{1})$ facet, which makes an angle of 34.5° with the $(20\bar{1})$ plane, the above expression becomes:

$$\Delta G = 1.63 \times \cos 34.5^{\circ} - 2.21 \cong -0.87(J\,m^{-2}) \quad (2)$$

Thus the $(20\bar{1})$ surface appears to be stable with respect to the formation of microscopic $(1\bar{1}\bar{1})$ facets, which is consistent with what had previously been found for stoichiometric SnO_2 nanoribbon growth.[10] It is conjectured that as the sample was cooled down without a sufficient supply of oxygen, there is a change in composition, bonding state, and/or surface relaxation, which may influences the surface energy. In addition, the variation in catalyst/SnO_2 interface energy may also play a role in the growth of the beaklike structure. Further investigations are required to clarify the growth mechanism.

Room-temperature PL measurements (Figure 5) show that the beaklike nanorods, in comparison with SnO_2 nanorods of uniform diameter (PL peak: 620 nm), exhibit a

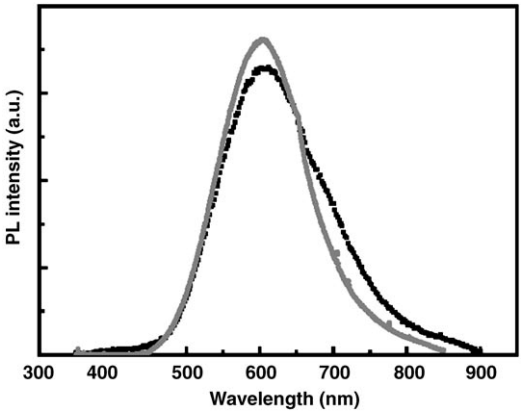

Figure 5. The photoluminescence spectra of beaklike SnO_2 nanorods (black) and nanorods of uniform diameter (grey).

slightly blue-shifted PL peak, centered at 602 nm. The strong PL peak might be related to the crystalline defects induced during the growth. The oxygen vacancies interact with interfacial tin vacancies, and lead to the formation of a considerable amount of trapped states within the bandgap, which results in a strong PL signal. Similar results were also observed for SnO_2 nanobelts.[13] On the other hand, direct comparison of the two sets of data cannot lead to the conclusion that the SnO_2 nanorods possess more oxygen deficiencies since the volume fraction of the nanorods are different and the defect structure of the beaklike tips and the main rods may also vary.

Nanorods are ideal objects for electron field emission (FE). Figure 6 shows the FE current density as a function of the applied field in a current density–electric field *(J–E)* plot and a $\ln(J/E^2)$–$1/E$ plot of the SnO_2 nanostructures. Comparing the *J–E* plots, all of the SnO_2 samples have excellent turn-on voltage values. The turn-on field (defined as the electric field required to generate a current density of 0.01 $mA\,cm^{-2}$) for the SnO_2 nanorods with uniform diameters (Figure 4a and b) was found to be about 6.4 $V\,\mu m^{-1}$, as shown in Figure 6a. Measurements on the beaklike SnO_2 nanorods (Figure 6b) show a turn-on field of 5.8 $V\,\mu m^{-1}$. Although these values of turn-on field are higher than the best

NANO MICRO small

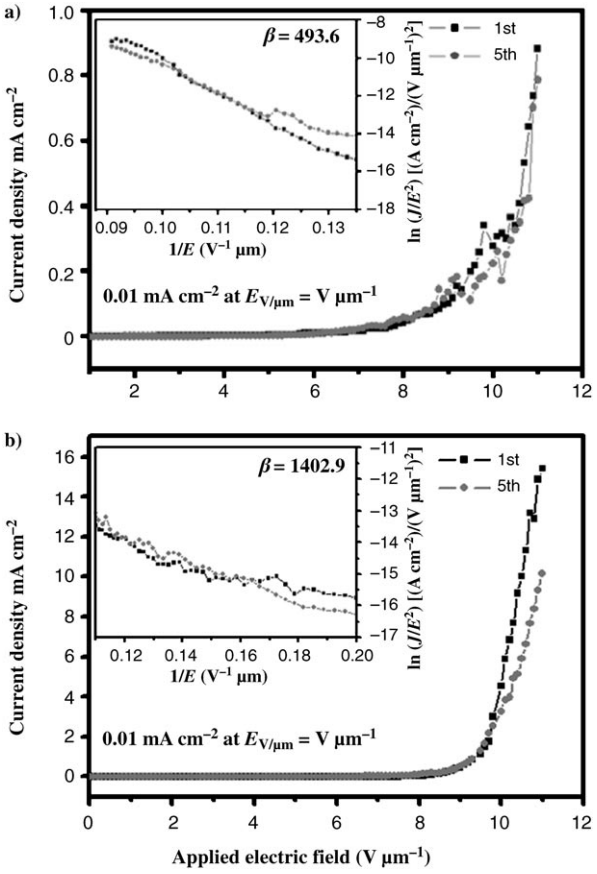

Figure 6. Field-emission current density versus electric field (J–E) for a) SnO_2 nanorods with a uniform diameter, and b) beaklike SnO_2 nanorods (the labels "1st" and "5th" signify that the data recorded were collected after the first and fifth experiments of a series, respectively). The insets show the corresponding Fowler–Nordheim relationship by way of a $\ln(J/E^2)$–$1/E$ plot .

data from carbon nanotubes[19] and SiC,[20] they are much lower than many other types of emitters such as carbon nitride,[21] Si nanostructures,[22] MoO_3 nanobelts,[23] and ZnO nanowires.[24,25] In general, FE current depends on the work function and geometry of the sample.[26] Based on the Folwer–Nordheim (FN) model, FE current from a metal or semiconductor is attributed to the tunneling of electrons from the material into vacuum through a potential barrier under the influence of an electric field.[27] In order to understand the FE behavior, the J–E data are also analyzed by applying the FN equation:

$$J = (A\beta^2 E^2/\Phi)\exp(-B\Phi^{3/2}/\beta E) \quad (3)$$

where J is the current density, E is the applied electric field, and Φ is the work function. A and B are constants, corresponding to 1.56×10^{-10} [$AeVV^{-2}$] and 6.83×10^{3} [$eV^{-3/2}(\mu m^{-1})$], respectively. The FN plot is shown in the insets in Figure 6. For a comparison, by determining the slope of the $\ln(J/E^2)$–$1/E$ plot with a work function value for SnO_2 of 4.7 eV,[28] the field-enhancement factor, β, can be calculated to be about 493.6 and 1402.9 for SnO_2 nanorods of uniform diameter and with a beaklike strucutre, respectively. As a result, the beaklike SnO_2 nanorods possess a much higher β value than the SnO_2 nanorods of uniform diameter. These comparative results have demonstrated that SnO_2 nanorods with a high aspect ratio possess excellent FE performance.

3. Conclusions

In summary, beaklike SnO_2 nanorods were fabricated by the VLS method. The beaklike structure was formed as a result of controlling the growth conditions towards the end of the synthesis. Based on TEM characterization and theory of Wulff construction, it was concluded that the nanorods grow along a direction close to $[10\bar{1}]$ and the beak is formed by switching the growth direction to approximately $[1\bar{1}\bar{2}]$. Both PL and FE measurements have shown that the beaklike nanostructures lead to superb physical properties. The PL spectrum of such nanorods exhibit a strong emission peak at 602 nm. From determining the slope of the $\ln(J/E^2)$–(I/E) plot, the field enhancement factor β is determined to be about 1400, and the turn-on field is 5.8 V μm^{-1} (in comparison, nanorods of uniform size without beaklike structure show a field enhancement factor β is 494 and a turn-on field of 6.4 V μm^{-1}). This clearly shows that beaklike SnO_2 nanorods have a better FE performance than nanorods of uniform diameter. In addition, the shape and curved tips of the nanorods are important for determining the FE properties.

4. Experimental Section

Single crystal, 3–5 Ω cm, phosphorous-doped Si(001) wafers were used in this study. The silicon wafers were cleaned chemically by a standard RCA (Radio Corporation of America) cleaning process, which is the industry standard for removing contaminants from wafers before loading into an electron-beam evaporation system. The RCA cleaning procedure has three major steps used sequentially:

1) Organic clean: removal of insoluble organic contaminants with a H_2O:H_2O_2:NH_4OH (5:1:1) solution;

2) Oxide strip: removal of a thin silicon dioxide layer where metallic contaminants may accumulate as a result of step 1), using a H_2O:HF (50:1) solution;

3) Ionic clean: removal of ionic and heavy-metal atomic contaminants using a H_2O:H_2O_2:HCl (6:1:1) solution.

The tin oxide nanorods were grown by the vapor–liquid–solid process. A 2-nm-thick Au film was deposited at ≈5 × 10^{-6} Torr onto a Si substrate at room temperature, which serves as the catalyst for growing the nanowires. Then, Sn particles (0.5 g) were placed in an alumina boat. The boat was positioned in a quartz tube that was inserted into a horizontal alumina tube furnace, and the Si substrates with the Au catalyst layer were placed downstream at ≈20 mm distance from the Sn particles. After evacuation with a rotary pump to a pressure of 10^{-3} Torr, the furnace was heated from room temperature to 1080 °C at a heating rate of 5 °C min^{-1} under an Ar flow of 150 sccm. The samples were held at 1080 °C under a 150 sccm Ar carrier gas

and a 12.5 sccm oxygen gas flow for 1 h, and the chamber pressure was kept at 6.4 Torr. Two different types of samples have been prepared by changing the cooling conditions while the synthesis conditions were kept the same. The first set of samples was cooled down to room temperature with a 150-sccm Ar flow and a 12.5-sccm oxygen flow. The other set of samples was cooled to room temperature with only a 150-sccm Ar flow.

After the growth process, the resulting products were collected for phase identification by using grazing incidence X-ray diffractometry (GIXRD) with a fixed incident angle of 0.5°. The substrate-bound nanorods were mechanically scraped and sonicated in ethanol and then deposited on carbon-coated copper grids for transmission electron microscope (TEM) characterization. Morphological studies of the SnO_2 nanostructures were performed with a JEOL 2010 TEM operating at 200 kV and a JEOL JSM-6500 field-emission scanning electron microscope (SEM). High-resolution TEM (HRTEM) images were obtained by using a JEOL JEM-3000F field-emission TEM, with a point-to-point resolution of 0.17 nm, operating at 300 kV. The PL properties of the synthesized nanorods were studied at room temperature using a He-Cd laser in the spectral range of 350–800 nm with a wavelength of 325 nm as the excitation source. The FE measurements of the SnO_2 nanorods were carried out under vacuum (1×10^{-7} Torr) using a spherical stainless steel probe (1 mm in diameter) as an anode. The emission current is recorded on the level of nanoamperes. The distance between the anode and the surface of the emitting sample (cathode) is fixed at 100 μm. A more accurate description of the relationship between the turn-on field and the distance between the anode and the samples was described in a previous work.[29]

Acknowledgements

The research was supported by the Republic of China National Science Council Grant No. NSC 94–2215-E-007–018 and Ministry of Education Grant No. 91-E-FA04–1–4.

[1] *Nanowires and Nanobelts, Vol. I: Metal and Semiconductor* Nanowires (Ed.: Z. L. Wang), Kluwer Academic, New York, **2003**.
[2] *Nanowires and Nanobelts, Vol. II: Nanowires and Nanobelts of Functional Materials* (Ed.: Z. L. Wang), Kluwer Academic, New York, **2003**.
[3] Z. L. Wang, Z. C. Kang, *Functional and Smart Materials*, Plenum, New York **1998**.
[4] S. Ferrere, A. Zaban, B. A. Gsegg, *J. Phys. Chem. B* **1997**, *101*, 4490.
[5] E. Comini, V. Guidi, C. Malagu, G. Martinelli, Z. Pan, G. Sberveglieri, Z. L. Wang, *J. Phys. Chem. B* **2004**, *108*, 1882.
[6] S. Mathur, S. Barth, H. Shen, J. C. Pyun, U. Werner, *Small* **2005**, *1*, 713.
[7] Y. Zhang, A. Kolmakov, S. Chretien, H. Metiu, M. Moskovits, *Nano Lett.* **2004**, *4*, 403.
[8] E. Comini, G. Faglia, G. Sberveglieri, Z. W. Pan, Z. L. Wang, *Appl. Phys. Lett.* **2002**, *81*, 1869.
[9] Z. L. Wang, *Adv. Mater.* **2003**, *15*, 432.
[10] Z. R. Dai, J. L. Gole, J. D. Stout, Z. L. Wang, *J. Phys. Chem. B* **2002**, *106*, 1274.
[11] Y. Liu, J. Dong, M. Liu, *Adv. Mater.* **2004**, *16*, 353.
[12] Z. W. Pan, Z. R. Dai, Z. L. Wang, *Science* **2001**, *291*, 1947.
[13] J. Q. Hu, Y. Bando, Q. L. Liu, D. Golberg, *Adv. Funct. Mater.* **2003**, *13*, 493.
[14] S. V. Khare, S. Kodambaka, D. D. Jonson, I. Petrov, J. E. Greene, *Surf. Sci.* **2003**, *52*, 75.
[15] G. Wulff, *Z. Kristallogr. Mineral.* **1901**, *34*, 449.
[16] A. Beltrán, J. Andrés, E. Longo, E. R. Leite, *Appl. Phys. Lett.* **2003**, *83*, 635.
[17] J. Oviedo, M. J. Gillan, *Surf. Sci.* **2000**, *463*, 93.
[18] B. Slater, C. R. Catlow, D. H. Gay, D. E. Williams, V. Dusastre, *J. Phys. Chem. B* **1999**, *103*, 10644.
[19] A. M. Rao, D. Jacques, R. C. Haddon, W. Zhu, C. Bower, S. Jin, *Appl. Phys. Lett.* **2000**, *76*, 3813.
[20] Z. W. Pan, H. L. Lai, F. C. K. Au, X. F. Duan, W. Y. Zhou, W. S. Shi, N. Wang, C. S. Lee, N. B. Wong, S. T. Lee, S. S. Xie, *Adv. Mater.* **2000**, *12*, 1186.
[21] E. J. Chi, J. Y. Shim, H. K. Baik, S. M. Lee, *Appl. Phys. Lett.* **1997**, *71*, 324.
[22] T. Sugino, S. Kawasaki, K. Tanioka, J. Shirafuji, *Appl. Phys. Lett.* **1997**, *71*, 2704.
[23] Y. B. Li, Y. Bando, D. Golberg, K. Kurashima, *Appl. Phys. Lett.* **2002**, *81*, 5048.
[24] C. J. Lee, T. J. Lee, S. C. Lyu, Y. Zhang, H. Ruh, H. J. Lee, *Appl. Phys. Lett.* **2002**, *81*, 3648.
[25] Y. K. Tseng, C. J. Huang, H. M. Cheng, I. N. Lin, K. S. Liu, I. C. Chen, *Adv. Funct. Mater.* **2003**, *13*, 811.
[26] J. Chen, S. Z. Deng, N. S. Xu, S. Wang, X. Wen, S. Yang, C. Yang, J. Wang, W. Ge, *Appl. Phys. Lett.* **2002**, *80*, 3620.
[27] R. H. Fowler, L. W. Nordheim, *Proc. R. Soc. London Ser. A* **1928**, *119*, 173.
[28] T. Minami, T. Miyata, T. Yamamoto, *Surf. Coat. Technol.* **1998**, *108*, 583.
[29] C. C. Tang, D. Golberg, Y. Bando, F. F. Xu, B. Liu, *Chem. Commun.* **2003**, *24*, 3050.

Received: June 24, 2005
Revised: September 14, 2005

